Received May 2, 2022, accepted May 18, 2022, date of publication May 23, 2022, date of current version May 27, 2022.

Digital Object Identifier 10.1109/ACCESS.2022.3177661

Adaptive Synthetic Inertia Control Framework for Distributed Energy Resources in Low-Inertia Microgrid

SUMIT NEMA[1], (Student Member, IEEE), VIVEK PRAKASH[2], (Senior Member, IEEE), AND HRVOJE PANDŽIĆ[2], (Senior Member, IEEE)

[1]School of Automation, Banasthali Vidyapith, Tonk, Rajasthan 304022, India
[2]Faculty of Electrical Engineering and Computing, University of Zagreb, 10000 Zagreb, Croatia

Corresponding author: Vivek Prakash (vivekprakash@ieee.org)

This work was supported in part by the Croatian Science Foundation through the Project Active NeIghborhoods energy Markets pArTicipatION—ANIMATION under Grant IP-2019-04-09164.

ABSTRACT Bulk integration of Distributed Energy Resources (DERs) into the power grids reduces the system's inherent inertial response.The reduced inertial response causes a high Rate-of-Change-of-Frequency (RoCoF) and poses formidable operational challenges for the grid frequency stability. Interconnections around the world comprehend the role and value of the Synthetic Inertia Control (SIC), which is considered as a subset of the Fast Frequency Response (FFR) and as one of the potential solutions to arrest high RoCoF in low-inertia power systems. This paper proposes an intelligent SIC model with an adaptive Fuzzy Logic Controller for a low-inertia microgrid. The proposed Fuzzy-SIC (FSIC) design optimizes the DER output to fulfill the FFR requirements of the system for various operating conditions. The particle swarm optimization algorithm is applied to tune the SIC unit parameters along with the secondary Proportional-Integral-Derivative control. The proposed approach is examined in a control area with distinct degrees of DERs and load. Case studies and numerical results demonstrate about 87% improvement in RoCoF and frequency nadir in comparison to the system without a synthetic inertia emulation. Furthermore, the robustness of the proposed approach is evaluated using various case studies and a time-domain analysis is conducted to demonstrate the impact of incremental SIC parameters on the system parameters.

INDEX TERMS Distributed energy resources, dynamic frequency control, fast frequency response, fuzzy-logic, low-inertia microgrid, particle-swarm optimization, synthetic inertia.

NOMENCLATURE

β	Pitch angle (°)
Δf	Change in frequency (Hz))
$\dot{\Delta f}$	Rate of change of frequeny (Hz/s)
η	Conversion efficiency of the PV panels
λ	Tip ratio
ω	Rotational speed of blade (rad/s)
ρ	Air density (kg/m^3)
φ	Solar irradiance (kW/m^2)
A	Swept area of the blades (m^2)
C_p	Power coefficient of WTG
D	System damping coefficient(p.u./Hz)
D_{sie}	Synthetic damping coefficient of ESS (p.u./Hz)
D_{siw}	Synthetic damping coefficient of WTG (p.u./Hz)
H	Inertia constant (p.u. s)
H_{sie}	Synthetic inertia coefficient of ESS (p.u. s.)
H_{siw}	Synthetic inertia coefficient of WTG (p.u. s.)
K_d	Derivative gain of the secondary control (s)
K_i	Integral gain of the secondary control (s)
K_p	Proportional gain of the secondary control(s)
K_{sup2}	Supplementary controller gain of WTG
min	Minimum
max	Maximum
P_{deg}	Power output from DEG unit (p.u.)
P_{ess}	Power output from ESS unit (p.u.)
P_l	Change in load power(Disturbance) (p.u.)

The associate editor coordinating the review of this manuscript and approving it for publication was Youngjin Kim.

P_{pv}	Output power of the PV panels (p.u.)
P_{sic}	Power output from SIC unit (p.u.)
P_{wtg}	Power output from WTG unit (p.u.)
P_w	Output mechanical power of WTG (p.u.)
R	Radius of blades(m)
R_{sie}	Synthetic droop coefficient of ESS (Hz/p.u.)
S	Area of PV panels (m^2)
T_a	Ambient temperature (°C)
T_{inv}	Inverter time constant of the ESS (s)
V_w	Speed of the wind (m^2)

I. INTRODUCTION

High penetration of uncertain Distributed Energy Resources (DERs) such as wind and photovoltaics (PV) into the electric grid22 creates formidable challenges for the security and stability of the grid. DERs are interfaced through power electronic converters and are inherently incapable to fulfil the system frequency response requirements [1], [2]. Hence, to maintain the system frequency within a prescribed operating range and control the post-fault high Rate of Change of Frequency (RoCoF), the Synthetic Inertia Control (SIC) from DERs is envisaged as a solution [3]. The SIC is considered as a subset of Fast Frequency Response (FFR), which requires fast active power delivery within 2 seconds after the system frequency breaches the safe operating dead bands and should be maintained for at least 10 seconds [4]. SIC is an emulation of the inertial response from the source that is inherently incapable of delivering rotational kinetic energy as provided by the synchronous generators. The active power output of DERs can be controlled to mimic kinetic energy in response to a terminal frequency variation [5], [6]. Several research works have focused on the control of DERs such as Energy Storage System (ESS), Wind Turbine Generator (WTG), PV, Diesel Engine Generators (DEG), *etc.*, for frequency control [7]–[11]. In case of WTG and PV, the SIC design parameters require an additional power signal to pull away the PV or WTG from its maximum power operating point. In case of frequency deviation, the SIC activation starts, and additional active power is produced [12], [13]. The impact of synthetic inertia provision from PV systems on RoCoF and frequency nadir improvement has been observed in specific systems, *e.g.* [14]. The SIC parameters such as droop, damping, and the inverter time constant impact on the system frequency response performance, are observed in [15], [16]. It is concluded that hard bounds on the SIC parameters result in delayed response to reach a steady-state condition. Most controllers consider droop control and Load Frequency Control (LFC) to arrest and stabilize frequency deviations [17].

Various computational algorithms and intelligent controllers are investigated for the improvement in topology, schemes, and parameters for SIC [18]. An LFC design is proposed in [19]. A multi-area frequency control using adaptive FLC is described in [20], while the real-time application under high wind penetration is discussed by [21]. The work in [22] extends the frequency control using the adaptive fuzzy droop and fuzzy observer integrated into the power system. The studies conducted in [17]–[22] based on FLC have shown improvements in controllers, system design, application, and their role to stabilize the system. However, the coordinated DERs control strategies in providing FFR control under the condition of high RoCoF in low-inertia microgrids still require wider investigation. Table 1 provides the system specific comparison of existing research with proposed SIC strategy.

TABLE 1. System specific comparison of proposed work with existing research.

Ref.	RE (%)	Adaptive	FR	RoCoF (Hz/s)	Freq. Nadir (Hz)	Steady State Freq. (Hz)
[3]	20-80	No	PFR	-	-	-
[5]	10-40	No	PFR	-	-	-
[10]	upto 20	No	PFR	-	-	49.7-50.3
[12]	12-30	No	PFR	less than 1	48.4-48.7	49.58-49.75
[13]	10	Droop	PFR	4	49.88-49.93	-
[19]	20-80	Yes	PFR	-	49-51	49.5-50.5
Proposed work	**40-80**	**Yes**	**FFR**	**less than 1**	**49.5-50.5**	**49.8-50.2**

In [23], the function and utility of ESS with inverter control is evaluated for FFR capabilities. Studies on the appropriate ESS size and estimation of optimal parameters to replicate the Synthetic Inertia (SI) are, however, restricted, [24], [25].The ESS modest size may not be enough to achieve the required inertia, while a bigger scale may result in higher investment and operations costs. Furthermore, the DER emulated inertia provision must include a self-adaptability or flexibility feature for real-time variations in FFR requirements [26]–[28]. Hence, this calls for a SIC framework that considers the FFR requirement variation and provides a rapid response according to the change in RoCoF and frequency nadir.

In the context of the discussed research challenges, this paper develops a novel coordinated SIC control provision from DERs, *i.e.* WTG, PV, ESS with an inverter, and DEG for a low-inertia microgrid. The proposed SIC model contains multiple variables that are optimized to arrest high RoCoF and frequency deviations following a large disturbance. The Particle Swarm Optimization (PSO) metaheuristic technique is used to optimize the optimal response of the DER along with the required SIC and the secondary Proportional-Integral-Derivative (PID) controller parameters. Furthermore, Fuzzy-SIC (FSIC) strategy is developed to incorporate the self-adaptive capability into the proposed model under several disturbances or load variations. The proposed SIC controller is tested in various case studies to emulate the adaptive SI response considering the frequency deviations and RoCoF.

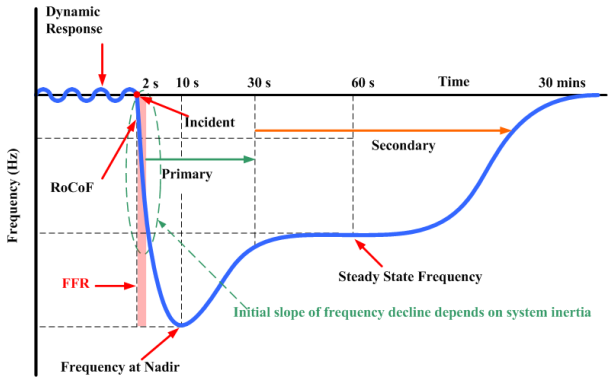

FIGURE 1. Frequency response curve after a contingency event.

To address the outlined research challenges, the main contribution of this paper consists of the following:

1) Formulation of an intelligent adaptive FSIC framework for low-inertia microgrids mapped with FFR requirements and frequency security constraints, *i.e.*, frequency deviations and RoCoF.

2) Identification of optimal DER capacity for the SI response and optimization of various SIC and PID parameters (inertia coefficients, droop coefficients, inverter time constant, controller's gain) for FFR and secondary frequency control.

3) Assessment of the feasibility of the proposed FSIC strategy for the improvement in the frequency security parameters, *i.e.*, RoCoF and frequency nadir, under different disturbance conditions.

This paper is organized as follows: Section II discusses the fundamental modelling of the system inertia and the proposed SIC strategy. In Section III, the DER design parameters, the low-inertia microgrid configuration, the intelligent adaptive FSIC, and the PSO algorithm strategy are described. Section IV highlights various cases with several combinations of DERs and applied disturbances. It further discusses the robustness of the proposed intelligent adaptive FSIC in terms of controlling RoCoF and frequency nadir. Finally, relevant conclusions are discussed in Section V.

II. ROLE AND VALUE OF INERTIAL RESPONSE

Inertial response is an inherent property of conventional generators, which allows for automatic rotational speed modulation based on the system frequency deviation. The kinetic energy stored in the spinning masses can be utilized to adjust the active power output according to its consumption to maintain frequency stability [29]. Since renewable energy generators lack spinning masses, the inertia of modern power grids will decrease significantly by replacing the existing synchronous generators with these power-electronics-controlled generators. Eventually, this issue of inertia will undermine the power system stability and reliability [30], [31]. Fig.1 shows a dynamic response of the system frequency for different time-scale including FFR.

A. INERTIAL RESPONSE MODELING OF TRADITIONAL GENERATORS

The equivalent rotating mass of all synchronous generators with equivalent inertia H_{eq} can be written as [32]:

$$H_{eq} = \frac{\sum_{i=1}^{n} H_i \cdot S_{base,i}}{S_{base}} \tag{1}$$

where n is the number of committed generators. The emulated inertial response stemming from the DERs is a part of the overall system inertia. The overall system inertia is comprised of the synchronous inertia stemming from conventional generators and the SI provision from DERs. as given by Eq. (2).

$$H_{eq} = \frac{\overbrace{\sum_{i=1}^{n} H_i \cdot S_{base,i}}^{Conventional} + \overbrace{\sum_{j=1}^{m} H_j \cdot S_{base,j}}^{RES}}{S_{base}} \tag{2}$$

B. SYNTHETIC INERTIA CONTROL PROVISION FROM DERs

The SIC strategy is proposed to obtain a collective response from the DERs in a low-inertia microgrid [2], [3]. Fig. 2 illustrates the dynamic structure of the SIC model, consisting of an ESS with an inverter, a DEG, a WTG, and a PV with an inertial control scheme that synthesizes the inertia and damping by managing the active power. The SIC must absorb or feed in active power for the required inertia compensation. Here, the State-of-Charge (SOC) for the ESS could be defined by its nominal capacity (steady state). The simulated power from a SIC unit may be expressed as follows:

$$P_{sic} = P_{wtg} + P_{ess} \tag{3}$$

The active power contribution for FFR through WTG can be given by:

$$P_{wtg} = P_w + P_{droop} \tag{4}$$

where P_w is the output mechanical power defined in Eq. (7) and P_{droop} can be written as follows:

$$P_{droop} = P_{hw} + P_{dw} + P_{kw} \tag{5}$$

Here, P_{hw}, P_{dw}, and P_{kw} are the output power variables corresponding to H_{siw}, D_{siw}, and K_{sup2}. In Eq. (3), P_{ess} is the output power of the ESS obtained through the inverter defined as follows:

$$P_{ess} = \frac{sH_{sie} + D_{sie}}{1 + sT_{inv}} \left(\frac{\Delta f}{R_{sie}} \right) \tag{6}$$

III. METHODOLOGY

A. MODELING OF DERs IN ISOLATED MICROGRID

In this paper, a dynamic model of a low-inertia islanded microgrid is developed to perform an FFR analysis regarding SIC from various DERs.

1) DIESEL ENGINE GENERATOR

The DEG is a quick source of power generation and can serve a load increment with high sturdiness. The DEG can generate electrical power according to the grid requirement. The power output of a DEG can be altered based on the load variation. The DEG transfer function for SIC is shown in Fig. 2.

2) WIND TURBINE GENERATOR

The WTG is designed as a power variation resource for the considered low-inertia microgrid. The model is based on the steady-state power characteristics of the turbine. The output mechanical power of WTG is given by Eq. (7) as follows [10]:

$$P_w = \frac{1}{2}\rho A C_p(\lambda, \beta) V_w^3 \tag{7}$$

Here, $\rho = 1.25\ \text{kg/m}^3$ and $A = \pi R^2$ is the swept area of the blades in m^2. The WTG output power can be specified as a mix of the power coefficient C_p and also various other physical elements. Tip ratio λ can be obtained as:

$$\lambda = \frac{R \times \omega_{\text{blade}}}{V_w} \tag{8}$$

where $\omega = 3.14$ rad/s. A generic equation is used to model $C_p(\lambda, \beta)$. This equation, based on the turbine modeling characteristics of [33], is:

$$C_p(\lambda, \beta) = C_1 \left(C_2/\lambda_i - C_3\beta - C_4\right) e^{-C_5/\lambda_1} + C_6\lambda \tag{9}$$

$$\frac{1}{\lambda_i} = \frac{1}{\lambda + 0.08\beta} - \frac{0.035}{\beta^3 + 1} \tag{10}$$

The coefficients C_1 to C_6 are: $C_1 = 0.5176, C_2 = 116$, $0.4, C_4 = 5, C_5 = 21$ and $C_6 = 0.0068$ [34].

3) PV PANELS

The output power of the PV panels is determined by:

$$P_{pv} = \eta \times S \times \varphi \times (1 - 0.005\,(T_a + 25)) \tag{11}$$

where η ranges from 7% to 19% [35]. φ is kept at $1\ \text{kW/m}^2$ [19]. From Eq. (11), the value P_{pv} depends on the solar irradiance as the parameters S and η are constant. To design a PV module, a single diode model is considered [22]. A 100 kW PV plant is designed where each PV can deliver up to 305 W, having an open-circuit voltage $V_{oc} = 64.2$ V and short-circuit current $I_{sc} = 5.96$ A.

4) DER COORDINATION

A coordinated operation of the SIC with the ESS supervises the additional injection of power with suitable inertia and damping coefficients after a disturbance. The primary control must balance the system frequency to a new steady-state value within a specified time frame. The frequency deviation of an islanded microgrid is represented by linearizing the dynamic effects of the load-generation blocks, which include the SIC, the primary control loop, and the secondary control loop, as illustrated in Fig. 2.

$$\Delta f(s) = \frac{1}{2Hs + D}\left(P_{deg}(s) + P_{sic}(s) + P_{pv}(s) - P_l(s)\right) \tag{12}$$

TABLE 2. Microgrid parameters.

Parameter	Value	Parameter	Value	Parameter	Value
D (p.u./Hz)	0.015	T_{wtg}(s)	2	$T_{inertia-De}$ (s)	0.1
$2H$ (p.u. s)	0.1667	T_g (s)	0.8	T_{M-De}(s)	0.01
R (Hz/p.u.)	2	T_t(s)	0.4		

A metaheuristic PSO is implemented to obtain the parameters of the PID controller (secondary control loop). A small-signal model of the microgrid comprising conventional units and DERs with F-SIC unit is shown in Fig.2, while the relevant parameters are listed in Table 2.

B. PSO FOR SIC PARAMETER OPTIMIZATION

The PSO [36], [37] is used to optimize the SIC parameters due to its high computational efficiency, flexibility, and robustness of the control parameters [33]. The particle placement upgrade is recognized by utilizing *pbest*(personal best) and *gbest* (global best), which are the most effective fitness parameter of the j^{th} particle. After a specified iteration or a specified stopping condition, the ideal solution is established by the value of *gbest*. The position and velocity of the j^{th} particle are denoted as x_j and v_j, specific and global learning coefficients are termed as c_1 and c_2, while r_1 and r_2 are arbitrary numbers in the range from 0 to 1. The most effective and satisfactory outcome following the constraints defines the fitness of the objective function. Eqs. (13) and (14) are used to upgrade the velocity and position of the particles as follows:

$$v_{j,i+1} = w \cdot v_{j,i} + c_1 \cdot r_1 \left(\text{pbest}_j - x_{j.i}\right) + c_2 \cdot r_2 \left(\text{gbest}_j - x_{j.i}\right) \tag{13}$$

$$x_{j,i+1} = x_{j,i} + v_{j,i+1} \tag{14}$$

The objective function to determine the gains of PID controllers is taken as J_1 which is integral of the square value of Δf as complies with:

Minimize J_1

$$J_1 = \int_0^{t_{simulation}} (\Delta f)^2 dt \tag{15}$$

subject to:

$$K_p^{\min}, K_i^{\min}, K_d^{\min} \le K_p, K_i, K_d \le K_p^{\max}, K_i^{\max}, K_d^{\max} \tag{16}$$

The hybrid system is further optimized to determine parameters required for the SIC unit. Every possible setting represents a particle in the search space that changes its parameters, including the synthetic damping coefficients, the inverter time constant, and the supplementary control coefficient of the wind integrated droop control. In the proposed system, the ESS synthetic droop is also considered. To minimize Δf, a multi-objective function J_2, as the integral of the square of the frequency deviations, is considered. It minimizes over Δf, D_{siw}, K_{sup2}, R_{sie}, D_{sie} and T_{inv}.

Minimize J_2

$$J_2 = \int_0^{t_{simulation}} (\Delta f)^2 dt \tag{17}$$

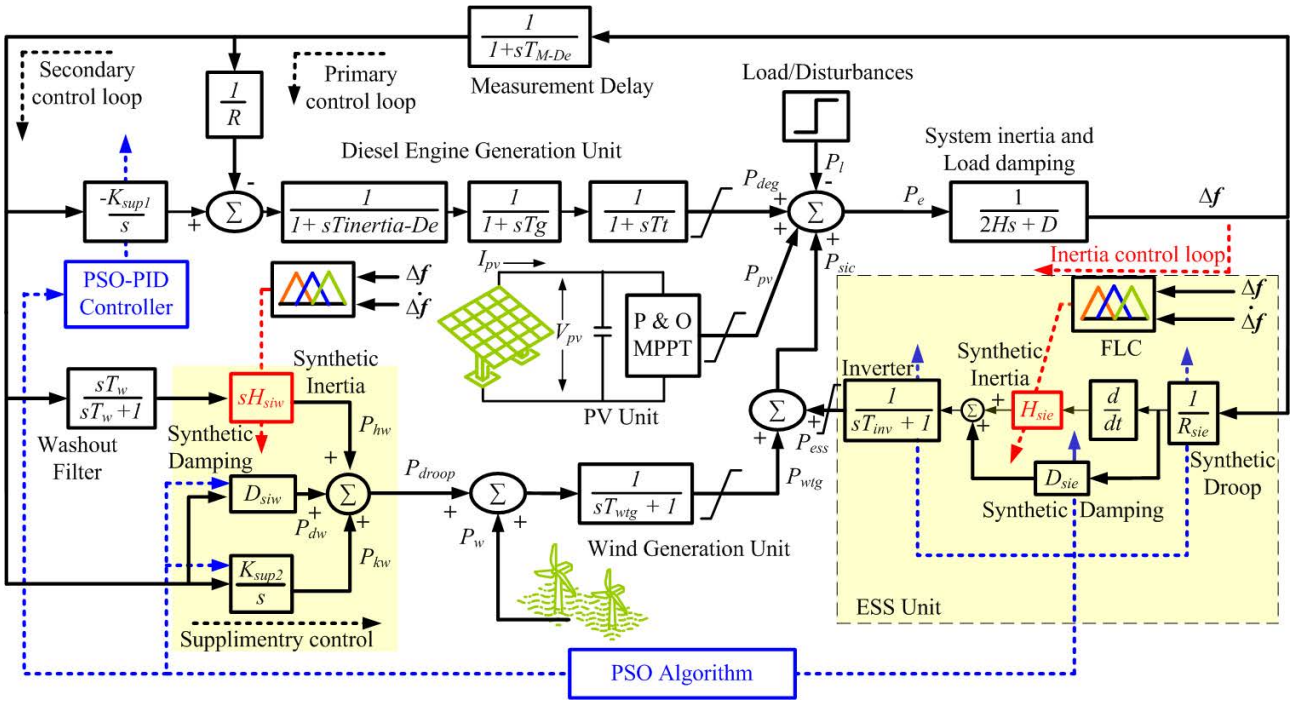

FIGURE 2. Dynamic frequency response model of the low-inertia microgrid with SIC scheme.

subject to:

$$\Delta f^{\min} \le \Delta f \le \Delta f^{\max} \tag{18}$$
$$D_{siw}^{\min} \le D_{siw} \le D_{siw}^{\max} \tag{19}$$
$$K_{sup2}^{\min} \le K_{sup} \le K_{sup2}^{\max} \tag{20}$$
$$R_{sie}^{\min} \le R_{sie} \le R_{sie}^{\max} \tag{21}$$
$$D_{sie}^{\min} \le D_{sie} \le D_{sie}^{\max} \tag{22}$$
$$T_{inv}^{\min} \le T_{inv} \le T_{inv}^{\max} \tag{23}$$

Optimization parameters for the PSO are as follows: maximum iterations = 15; swarm size = 50; inertia weight = 0.729; $c_1 = 1.5$ and $c_2 = 2$. Objective functions J_1, and J_2 are minimized for $|\Delta f| = 0.2$ Hz. The minimum and maximum ranges for constraints are D_{siw}:[0,435], K_{sup2}:[0,360], R_{sie}:[0.1,0.3], D_{sie}:[0,0.4] and T_{inv}:[0.1,1]. The generalized flow of the optimization algorithm is depicted in Fig.3, while the fitness of both objective functions is presented in Fig.4.

C. FUZZY-SIC (FSIC) STRATEGY

The FLC system, also referred to as an intelligent control system, is widely used in various fields [18]. An advantageous feature of the FLC is being able to provide an optimal solution with low training data. It can provide flexibility and optimal solutions for imprecise and incomplete data, nonlinear disturbances, and uncertainty. A general structure of the FLC system is shown in Fig. 5 [33], [38]. The fuzzy controller inputs are the crisp values of RoCoF and frequency deviation. The FLC outcome is a normalized crisp value. First, the preprocessing is executed to change the dimension of scale inputs. Then, the fuzzification is carried out to modify the real

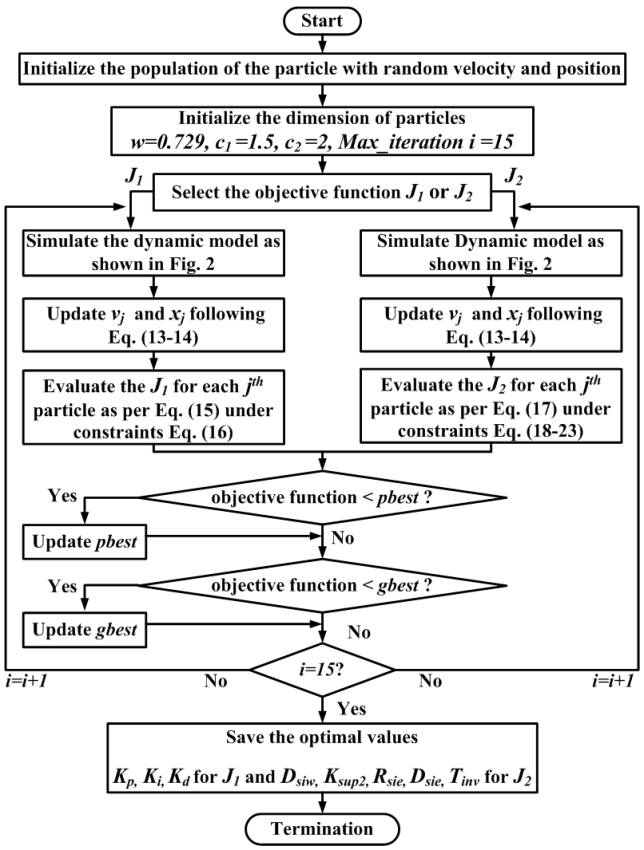

FIGURE 3. PSO algorithm for SIC parameter optimization.

inputs to the fuzzy values. The Mamdani [39] reasoning is used in the interface procedure. Inputs 1 and 2 are created as:

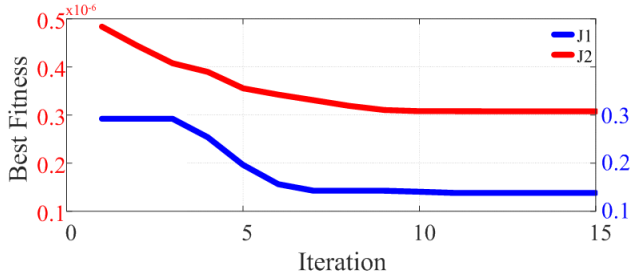

FIGURE 4. Fitness plot of objective functions J_1 and J_2.

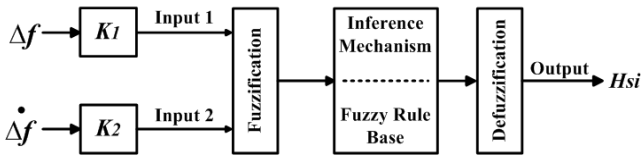

FIGURE 5. Dynamic structure for the fuzzy logic scheme.

$Input\,1 = \Delta f \cdot K_1$ and $Input\,2 = \dot{\Delta f} \cdot K_2$. Input signals Δf and $\dot{\Delta f}$ are merged and fuzzy rules are implemented to determine optimal H_{sie} and H_{siw} values. An inference connection C, as defined in Eq. (24), can be obtained from the knowledge base developed by the database and the rules. The database includes a summary of input as well as output variables making use of fuzzy sets [40]. The rules base is the control approach of the system. K_1 and K_2 are scaling factors with values $K_1 = K_2 = 1$.

$$C^{(j)} : \text{IF } i_1 \text{ is } F_1 \text{ and } i_2 \text{ is } F_2 \ldots i_n \text{ is } F_n \quad \text{THEN Y is } D^{(j)}, j = 1, \ldots, m \tag{24}$$

where $i_1, i_2 \ldots i_n$ is the input vector, Y is the output vector, while $D^{(j)}$ is the control output, n refers to the number of fuzzy variables, m is the number of rules, and $(F_1, F_2 \ldots F_n)$ is defined as a fuzzy set. Various Membership Functions (MFs) for the input and output of the FSIC are proposed in Fig. 6. In this work seven MFs are considered for inputs and output. This is because more number of fuzzy sets allow to capture and segregate the input into different classifications and gives a response with a high resolution. Both the inputs and output have two trapezoidal and five triangular MFs. The operating range of fuzzy input variables are Δf : $[-0.2, 0.2]$ and $\dot{\Delta f}$: $[-0.2, 0.2]$, while the ranges of H_{sie} and H_{siw} are $[0, 0.3]$ and $[30, 37]$, respectively. The bounds ranges were determined by internal model control technique [41]. The grade of every membership is signified by μ. Linguistic variables defined for the input and output fuzzy subsets are as follows: NL is negative large, NM is negative medium, NS is negative small, Z is zero, PS is positive small, PM is positive medium, and PL is positive large. The applied rule can be read as 'if Δf is NL and $\dot{\Delta f}$ is NL, THEN Y is PL'.

The rules of FSIC are created by determining the operational points $(P_1 - P_6)$ and area $(A_1 - A_4)$ of the dynamic response using the conventional control, as shown in Fig.7. When Δf and $\dot{\Delta f}$ are negative, *i.e.* area A_1, P_e is negative,

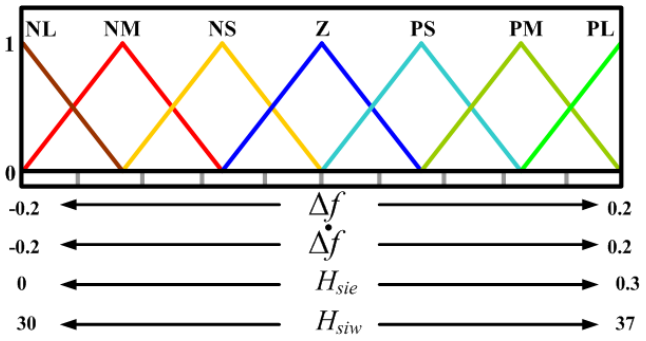

FIGURE 6. MFs of input and output variable.

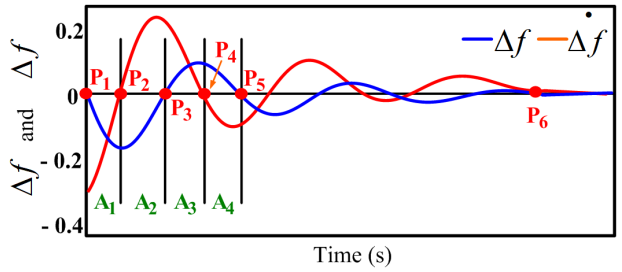

FIGURE 7. Dynamic system response to construct fuzzy rules.

implying $P_l > P_{\text{sic}}$, indicating a decrease in the system inertia. Therefore, to make P_e (power error) or Δf zero, the emulated inertia *i.e.*, SI should be positive. Hence Y will be positive, as a result, rules 1, 2, 3, 8, 9, 10, 15, 16, and 17, as shown in Table 4, get activated. Whenever the responses Δf and $\dot{\Delta f}$ are zero, *i.e.*, point P_6, Y will be constant or zero (will depend upon the system requirement and design strategy). As a result, Rule 25 is necessary to keep the steady-state error response stable and zero. The remaining rules are built the same way, using Fig. 7 and Tables 3 and 4. The fuzzy linguistic output is obtained by the fuzzy inference mechanism using the rules. The results obtained from the rules are forwarded for defuzzification. The modified crisp value is obtained as:

$$H_{si} = \frac{\sum_{j=1}^{n} x_i \cdot \mu(x_i)}{\sum_{j=1}^{n} \mu(x_i)} \tag{25}$$

Using Eq. (25), H_{sie} and H_{siw} are obtained using the proposed control algorithm and MFs. Hence, the proposed fuzzy-based SIC offers adequate inertia with self-adaptive capability from the ESS. An ESS, such as a battery, would be required for both the SIC and frequency droop management to deliver continuous active power in response to a grid frequency deviation [42]. Additionally, it provides low-frequency rapid damping, which results in the overshoots/undershoot occurred by integrating the DERs at different penetration levels, as well as load levels.

IV. SIMULATION RESULTS AND ANALYSIS

A dynamic model of a low-inertia microgrid is developed without and with a SIC unit. The parameters of the microgrid

TABLE 3. Fuzzy rule criteria.

	P_1	A_1	P_2	A_2	P_3	A_3	P_4	A_4	P_5	P_6
Δf	0	Negative	Negative	Negative	0	Positive	Positive	Positive	0	0
$\dot{\Delta f}$	Negative	Negative	0	Positive	Positive	Positive	0	Negative	Negative	0
Y	Positive	Positive	Positive	Positive/0/Negative	Negative	Negative	Negative	Positive/0/Negative	Positive	0

TABLE 4. Rule base for FSIC.

Y \ Δf	NL	NM	NS	Z	PS	PM	PL
NL	1 PL	8 PL	15 PL	22 PM	29 PM	36 PS	43 Z
NM	2 PL	9 PM	16 PM	23 PM	30 PS	37 Z	44 NS
NS	3 PL	10 PM	17 PS	24 PS	31 Z	38 NS	45 NM
$\dot{\Delta f}$ Z	4 PM	11 PM	18 PS	25 Z	32 NS	39 NM	46 NM
PS	5 PM	12 PS	19 Z	26 NS	33 NS	40 NM	47 NL
PM	6 PS	13 Z	20 NS	27 NM	34 NM	41 NM	48 NL
PL	7 Z	14 NS	21 NM	28 NM	35 NL	42 NL	49 NL

A1, A2, A3, A4, P1, P2, P3, P4, P5, P6

TABLE 5. DER power ratings.

DER	Rated Power(kW)	Rated Power(p.u.)	Load(p.u.)
Wind	800	0.8	
PV	100	0.1	Varying Load
Diesel	160	0.16	0.2-0.8
ESS	40	0.04	

TABLE 6. Optimized PID controller gain.

K_p	K_i	K_d
4.698	4.983	2.964

are provided in Table 5. Optimal parameters of the PID controller are evaluated from the Eqs. (15) and (16) using PSO as given in Table 6. The dynamic model of the hybrid microgrid with a SIC unit is modeled, and the coefficients of the SIC unit are obtained to minimize the frequency deviation and RoCoF according to Eqs. (17)-(23). The optimality of the parameters obtained for dynamic performance is also verified by the Firefly Algorithm (FA) [43] for the same no. of populations and iterations. FA utilizes the flashing light of fireflies that be can be formulated in such a way that it is associated with the objective function to be optimized. The details can be found in [43]. The parameters for FA are: no. of population = 50, iterations = 15, Light Absorption Coefficient = 1, Attraction Coefficient Base Value = 2, Mutation Coefficient = 0.2, Mutation Coefficient Damping Ratio = 0.98. The coefficients of the optimized SIC unit are listed in Table 7. The MATLAB/Simulink platform was used for the modelling and analysis.

The output power of the PV corresponding to Eq.(11) for varying temperatures, as well as variable irradiance using boost converter topology through MPPT, is shown in Fig.8. The PV power generation is considered with a constant irradiance of 1000 W/m^2 at a constant temperature of 25°C. The dynamic performance of the system was tested for three different cases.

TABLE 7. Optimized SIC unit coefficient.

Parameter	Value (PSO)	Value (FA)
D_{siw} (p.u./Hz)	433.8	435
D_{sie} (p.u./Hz)	0.30	0.39
K_{sup2} (s)	358.9	357.4
T_{inv} (s)	0.80	0.70
R_{sie}(Hz/p.u.)	0.26	0.24

A. CASE I

In this study, the proposed system is simulated for three different conditions. The simulation time of 100 s and the participation of the DEG, the ESS, the WTG (4 units), and the load are considered. Step disturbances of 0.2 p.u. and 0.5 p.u. are applied at 0 s and 40 s. Further, the subsystem contains the DEG, the WTG (8 units), the PV, and the load. Step disturbances of 0.2 p.u. and 0.6 p.u. are applied at 0 s and 40 s, respectively. The PV generates 0.1 p.u. at 0 s and 0.07 p.u. at 40 s. The system is further tested for a step disturbance of 0.6 p.u. and 0.8 p.u. at 0 s and 40 s, respectively. In this condition initially all WTG are assumed to be in operation, while 4 units are supposed to fail at 40 s. The PV power output at 40 s is 0.1 p.u. The dynamic performance of the system frequency is depicted in Fig. 9.

For large disturbance and high renewable penetration level, the applied control strategy is efficient and controls the deviations within the lowest time frame. The zoomed plot in Fig. 9 shows the steady-state frequency. Perturbations occur due to the fluctuations in the WTG and the PV power output. The corresponding SI response is delivered by the controller to rapidly stabilize the system. The graphical response depicts the improvement in the frequency deviations, the RoCoF, and the frequency nadir. The frequency security parameters without and with SIC are analyzed in detail in Table 8.

In Case I, the RoCoF is minimized, resulting in a sharp decline in the frequency nadir. Fig. 10 depicts the frequency security parameters and the corresponding improvement in the RoCoF and reduction in frequency nadir. Under the fixed operation of DEG and constant step load change, the SI requirement is also steady. On the other hand, variable RES power output results in variable SI to minimize the frequency deviations. FSIC provides the required variable SI to maintain

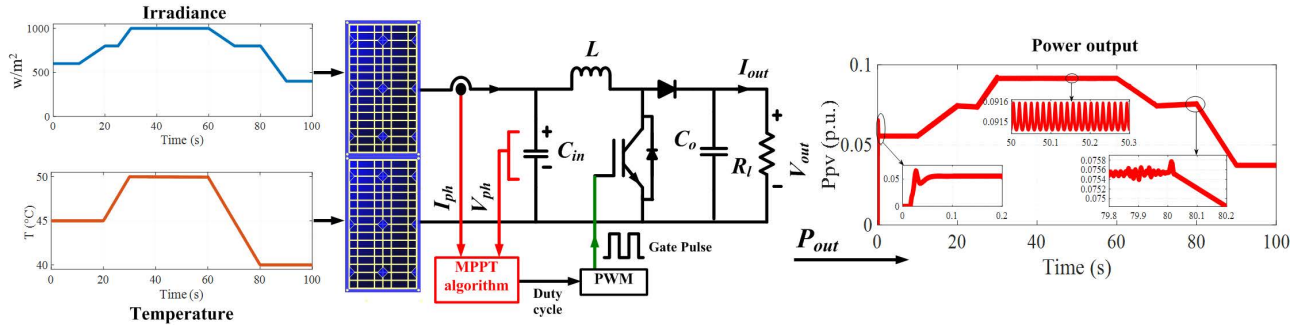

FIGURE 8. The output power of the PV unit.

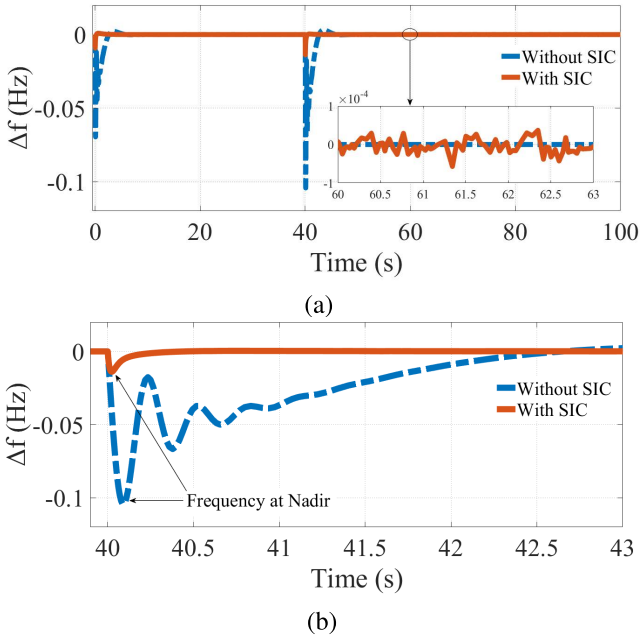

FIGURE 9. Δf for (a) 0-100 s and (b) zoomed plot for 40-43 s.

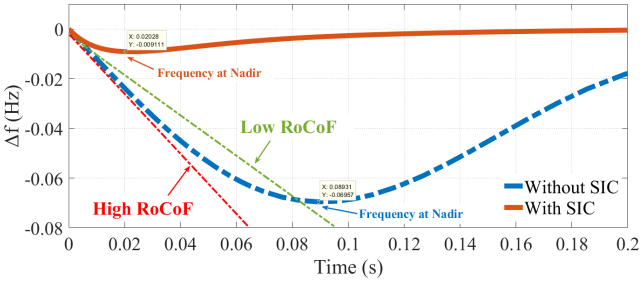

FIGURE 10. Improvement in RoCoF and frequency nadir.

the system stability. The SI response provided by the ESS and the WTG for Case I is shown in Fig. 11.

The self-adaptive feature of FSIC is analysed in comparison to a fixed value of the emulated inertia. The simulation time of 10 s is considered with step disturbance of 0.5 p.u. at 0 s. An individual comparative assessment for

TABLE 8. Frequency nadir improvement and RoCoF analysis for case I.

Subsystem with disturbance (p.u.)	Δf(Hz) without SIC	Δf(Hz) with SIC	% Improvement	Without SIC RoCoF (Hz)/(s)	With SIC RoCoF (Hz/s)
P_{deg}=0.16, P_{wtg}=0.4, P_{ess}=0.04 and P_l=0.2 (at 0 s)	0.069	0.009	86.84	0.77	0.40
P_{deg}=0.16, P_{wtg}=0.4, P_{ess}=0.04 and P_l=0.5 (at 40 s)	0.104	0.013	86.72	1.12	0.61
P_{deg}=0.16, P_{wtg}=0.8, P_{ess}=0.04, P_{pv}=0.1 and P_l=0.2 (at 0 s)	0.069	0.009	87.05	0.77	0.41
P_{deg}=0.16, P_{wtg}=0.8, P_{ess}=0.04, P_{pv}=0.07, and P_l=0.6 (at 40 s)	0.12	0.016	86.73	1.29	0.70
P_{deg}=0.16, P_{wtg}=0.8, P_{ess}=0.04, and P_l=0.6 (at 0 s)	0.06	0.009	87.05	0.77	0.41
P_{deg}=0.16,P_{wtg}=0.4, P_{ess}=0.04, P_{pv}=0.01, and P_l=0.2 (at 40 s)	0.17	0.023	86.53	1.99	0.97

H_{sie} = 0.01 and H_{siw} = 30.2 (obtained by the PSO) corresponding to FSIC scheme is shown in Fig. 12.

Since the power output of the PV and the WTG fluctuates, the system load conditions are variable. Therefore, the adaptive inertia rather than the fixed one should be emulated in the system to minimize the system frequency deviations. It is observed that the FSIC strategy is capable of rapidly arresting and stabilizing the frequency deviation as compared to the fixed SI capacity. The graphical results depict that lower frequency nadir and RoCoF can be achieved by adaptive FSIC.

B. CASE II

In this case, the system dynamic performance for 100%, 60%, and 40% of H and D parameters are analysed. The system is assumed to have lost its inertia and damping up to a certain level. A step disturbance of 0.2 p.u. is applied at 0 s and the obtained results are shown in Figs. 13 and 14.

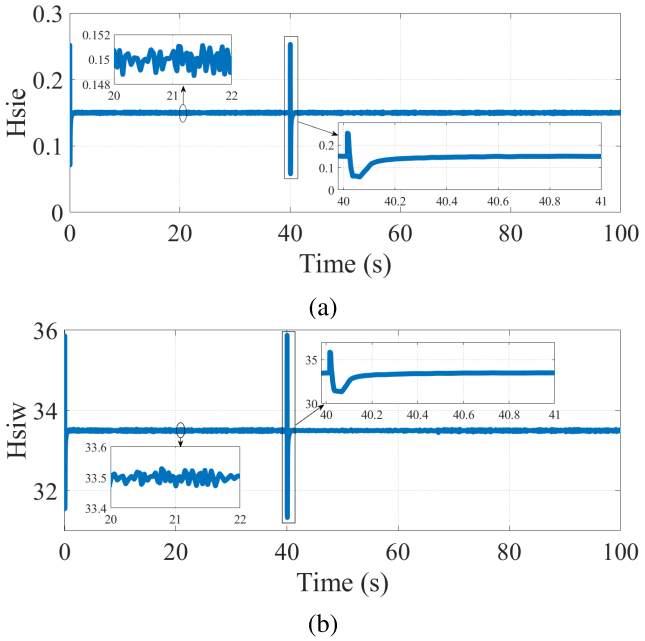

FIGURE 11. SI from (a) ESS (b) WTG for Case I.

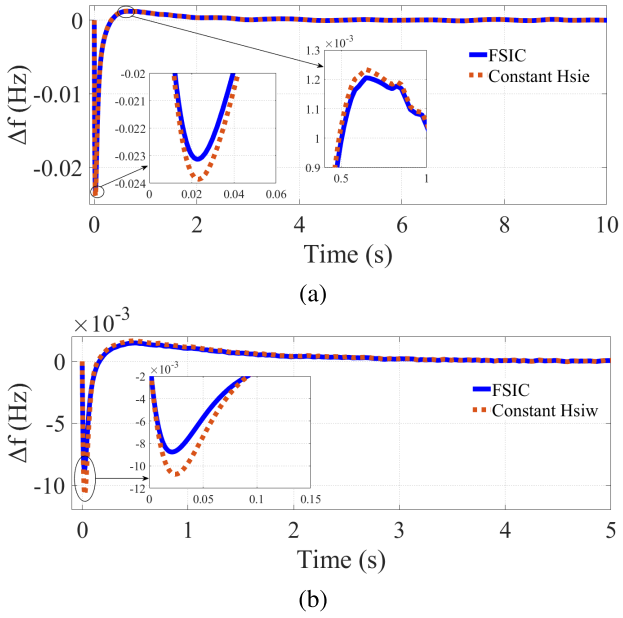

FIGURE 12. FSIC performance with (a) fixed H_{sie} (b) fixed H_{siw}.

There is a high-frequency nadir due to low system inertia and damping. However, the proposed FSIC scheme offers FFR and stabilizes the system frequency rapidly. The FSIC injects the required active power response into the system rapidly. Fig. 14 shows the emulated power required at low inertia and damping. The proposed controller possesses a higher injection rate as compared to the system condition.

C. CASE III

Unlike a real synchronous machine, the parameters of SIC can be attuned to improve the dynamic frequency response

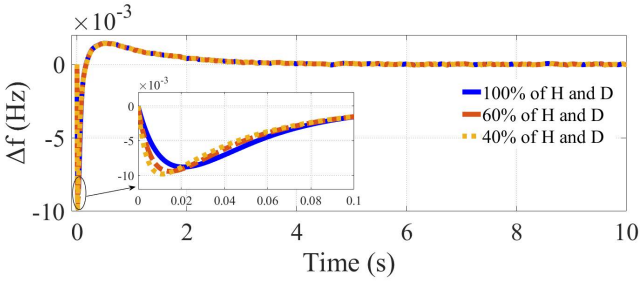

FIGURE 13. Frequency deviation with reduced *H* and *D*.

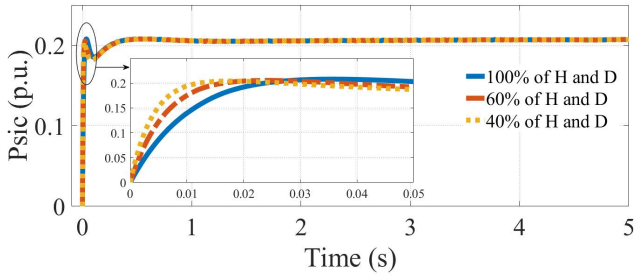

FIGURE 14. Dynamic response for reduced *H* and *D*.

TABLE 9. Impact of the SIC parameter on the system performance.

Parameter	H_{sie} (p.u. s)	D_{sie} (p.u./Hz)	R_{sie} (Hz/p.u.)	T_{inv} (s)
RoCoF	Decreases	Decreases	Decreases	Increases
Frequency Nadir	Lower	Lower	Lower	Raise
Overshoot	Increases	Decreases	Increases	Increases
Undershoot	Lower	Lower	Lower	Raise
Frequency Drop	Lower	Lower	Lower	Raise
Settling Time	Longer	Longer	Longer	Longer

of the system. In this case, the dynamic effects of SIC coefficients, specifically of the ESS, are investigated to achieve stable and robust performance of the system. The subsystem is composed of the DEG, the load, and the ESS-based FSIC. Simulation time is 20 s and a step disturbance of 0.2 p.u. is applied at 2 s. A comparative assessment of the system dynamics for different values of R_{sie}, D_{sie}, T_{inv} and H_{sie} of the ESS is observed as shown in Fig. 15. By reducing R_{sie}, the inverter-based ESS unit produces more inertia power with a faster response time. However, from Fig. 15.(a) the system response leads to a longer stabilization time following the disturbances. It is found that an increased H_{sie} results in a decreased system frequency nadir/ overshoot significantly, leading to an enhanced performance and stability of the system (Fig. 15.(b)). However, if H_{sie} is further increased, the system frequency would require a longer time to settle, resulting in a lower damping performance. To resolve this issue, D_{sie} may be increased for moderating an appropriate damping property and attaining an earlier stabilizing time. However, a large increase of D_{sie} causes a large overshoot effect. If D_{sie} is increased too much, an additional overshoot could occur. Fig. 15. (d) analyzes the system frequency response against the variations of T_{inv}. An increased T_{inv} causes high RoCoF

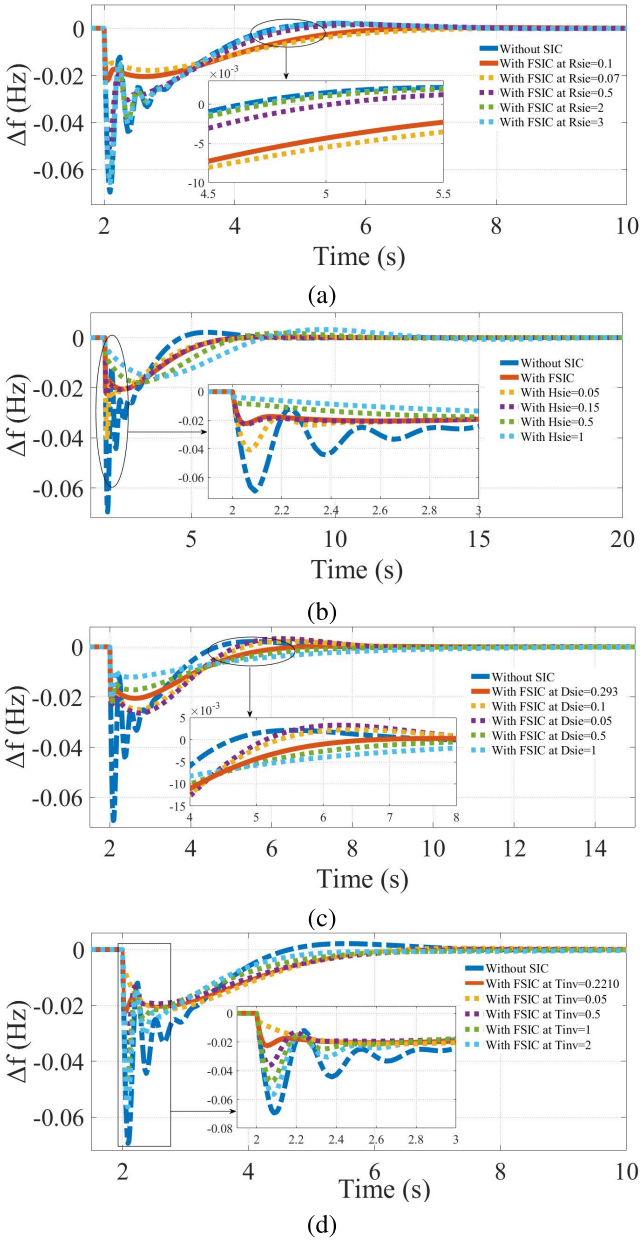

FIGURE 15. Δf **corresponding to variation in (a) Rsie, (b) Hsie, (c) Dsie and (d) Tinv.**

and frequency nadir. For a high value T_{inv}, the response time is slower than the conventional generating unit. The change in SIC parameters highlights the requirement of the optimal size of the DERs like ESS for the FFR provision. A detailed time-domain analysis for incremental changes in SIC coefficients is shown in Table 9.

V. CONCLUSION

This paper proposes an intelligent adaptive FSIC scheme and implements it to the dynamic model of a low-inertia microgrid. The proposed adaptive controller responds to the variation in frequency security parameters like RoCoF and frequency deviation and provides the required FFR by a coordinated control of DERs for different loading and operating conditions. The SIC and PID controller parameters are optimized in a manner to credibly respond to the abrupt disturbances in the presence of different levels of DER. It is observed that there is an 87% improvement in the system frequency dynamics performance for various disturbances and loading conditions as compared to the cases with no FSIC provision. This clearly shows the robustness of the proposed control scheme. Moreover, the dynamic performance of the system is analysed for the 100%, 60% and 40% inertia and damping adequacy. The simulation results and various case studies demonstrate the efficiency of the proposed SIC strategy and contribution of DERs, specifically the ESS, to the improvement in the SI response and the rapid frequency stability to counter the variability of the wind and PV power output. Furthermore, the impact of SIC parameter is analysed to showcase the improvement in the system performance parameters. The performance indices developed in this paper can strongly assist in the evaluation of the DER design parameters for the FFR with different operating conditions in low or zero-inertia grids.

REFERENCES

[1] K. S. Ratnam, K. Palanisamy, and G. Yang, "Future low-inertia power systems: Requirements, issues, and solutions—A review," *Renew. Sustain. Energy Rev.*, vol. 124, May 2020, Art. no. 109773.
[2] M. Dreidy, H. Mokhlis, and S. Mekhilef, "Inertia response and frequency control techniques for renewable energy sources: A review," *Renew. Sustain. Energy Rev.*, vol. 69, pp. 144–155, Mar. 2017.
[3] R. Eriksson, N. Modig, and K. Elkington, "Synthetic inertia versus fast frequency response: A definition," *IET Renew. Power Gener.*, vol. 12, no. 5, pp. 507–514, Apr. 2018.
[4] Q. Hong, M. Nedd, S. Norris, I. Abdulhadi, M. Karimi, V. Terzija, B. Marshall, K. Bell, and C. Booth, "Fast frequency response for effective frequency control in power systems with low inertia," *J. Eng.*, vol. 2019, no. 16, pp. 1696–1702, Mar. 2019.
[5] V. Prakash, P. Kushwaha, K. C. Sharma, and R. Bhakar, "Frequency response support assessment from uncertain wind generation," *Int. J. Electr. Power Energy Syst.*, vol. 134, Jan. 2022, Art. no. 107465.
[6] X. Zhao, Y. Xue, and X.-P. Zhang, "Fast frequency support from wind turbine systems by arresting frequency nadir close to settling frequency," *IEEE Open Access J. Power Energy*, vol. 7, pp. 191–202, 2020.
[7] J. Van de Vyver, J. D. M. D. Kooning, B. Meersman, L. Vandevelde, and T. L. Vandoorn, "Droop control as an alternative inertial response strategy for the synthetic inertia on wind turbines," *IEEE Trans. Power Syst.*, vol. 31, no. 2, pp. 1129–1138, Mar. 2015.
[8] R. K. Subroto, K. L. Lian, C.-C. Chu, and C.-J. Liao, "A fast frequency control based on model predictive control taking into account of optimal allocation of power from the energy storage system," *IEEE Trans. Power Del.*, vol. 36, no. 4, pp. 2467–2478, Aug. 2021.
[9] D. Al Kez, A. M. Foley, N. McIlwaine, D. J. Morrow, B. P. Hayes, M. A. Zehir, L. Mehigan, B. Papari, C. S. Edrington, and M. Baran, "A critical evaluation of grid stability and codes, energy storage and smart loads in power systems with wind generation," *Energy*, vol. 205, Aug. 2020, Art. no. 117671.
[10] L. Miao, J. Wen, H. Xie, C. Yue, and W. J. Lee, "Coordinated control strategy of wind turbine generator and energy storage equipment for frequency support," *IEEE Trans. Ind. Appl.*, vol. 51, no. 4, pp. 2732–2742, Jul./Aug. 2015.
[11] J. Xiao, Y. Jia, B. Jia, Z. Li, Y. Pan, and Y. Wang, "An inertial droop control based on comparisons between virtual synchronous generator and droop control in inverter-based distributed generators," *Energy Rep.*, vol. 6, pp. 104–112, Dec. 2020.
[12] G. Delille, B. Francois, and G. Malarange, "Dynamic frequency control support by energy storage to reduce the impact of wind and solar generation on isolated power system's inertia," *IEEE Trans. Sustain. Energy*, vol. 3, no. 4, pp. 931–939, Oct. 2012.

[13] A. Abazari, H. Monsef, and B. Wu, "Coordination strategies of distributed energy resources including FESS, DEG, FC and WTG in load frequency control (LFC) scheme of hybrid isolated micro-grid," *Int. J. Electr. Power Energy Syst.*, vol. 109, pp. 535–547, Jul. 2019.

[14] S. I. Nanou, A. G. Papakonstantinou, and S. A. Papathanassiou, "A generic model of two-stage grid-connected PV systems with primary frequency response and inertia emulation," *Electr. Power Syst. Res.*, vol. 127, pp. 186–196, Oct. 2015.

[15] M. Bahloul and S. K. Khadem, "An analytical approach for techno-economic evaluation of hybrid energy storage system for grid services," *J. Energy Storage*, vol. 31, Oct. 2020, Art. no. 101662.

[16] T. S. Amorim, D. Carletti, and L. F. Encarnação, "Comparison of inverter controllers with synthetic inertia and harmonic compensation features," *Electric Power Syst. Res.*, vol. 197, Aug. 2021, Art. no. 107344.

[17] V. Gholamrezaie, M. G. Dozein, H. Monsef, and B. Wu, "An optimal frequency control method through a dynamic load frequency control (LFC) model incorporating wind farm," *IEEE Syst. J.*, vol. 12, no. 1, pp. 392–401, Mar. 2018.

[18] H. R. Chamorro, I. Riaño, R. Gerndt, I. Zelinka, F. Gonzalez-Longatt, and V. K. Sood, "Synthetic inertia control based on fuzzy adaptive differential evolution," *Int. J. Electr. Power Energy Syst.*, vol. 105, pp. 803–813, Feb. 2019.

[19] T. Kerdphol, F. S. Rahman, Y. Mitani, M. Watanabe, and S. Küfeoglu, "Robust virtual inertia control of an islanded microgrid considering high penetration of renewable energy," *IEEE Access*, vol. 6, pp. 625–636, 2017.

[20] T. Kerdphol, F. Rahman, and Y. Mitani, "Virtual inertia control application to enhance frequency stability of interconnected power systems with high renewable energy penetration," *Energies*, vol. 11, no. 4, p. 981, Apr. 2018.

[21] D.-A. Ciupageanu, L. Barelli, and G. Lazaroiu, "Real-time stochastic power management strategies in hybrid renewable energy systems: A review of key applications and perspectives," *Electr. Power Syst. Res.*, vol. 187, Oct. 2020, Art. no. 106497.

[22] M. Ramesh, A. K. Yadav, and P. K. Pathak, "Intelligent adaptive LFC via power flow management of integrated standalone micro-grid system," *ISA Trans.*, vol. 112, pp. 234–250, Jun. 2021.

[23] L. Su, X. Qin, S. Zhang, Y. Zhang, Y. Jiang, and Y. Han, "Fast frequency response of inverter-based resources and its impact on system frequency characteristics," *Global Energy Interconnection*, vol. 3, no. 5, pp. 475–485, Oct. 2020.

[24] K. S. El-Bidairi, H. D. Nguyen, T. S. Mahmoud, S. D. G. Jayasinghe, and J. M. Guerrero, "Optimal sizing of battery energy storage systems for dynamic frequency control in an islanded microgrid: A case study of Flinders Island, Australia," *Energy*, vol. 195, Mar. 2020, Art. no. 117059.

[25] B. Yang, J. Wang, Y. Chen, D. Li, C. Zeng, Y. Chen, Z. Guo, H. Shu, X. Zhang, T. Yu, and L. Sun, "Optimal sizing and placement of energy storage system in power grids: A state-of-the-art one-stop handbook," *J. Energy Storage*, vol. 32, Dec. 2020, Art. no. 101814.

[26] H. Shi, F. Zhuo, H. Yi, F. Wang, D. Zhang, and Z. Geng, "A novel real-time voltage and frequency compensation strategy for photovoltaic-based microgrid," *IEEE Trans. Ind. Electron.*, vol. 62, no. 6, pp. 3545–3556, Jun. 2015.

[27] C. Ziras, E. Vrettos, and S. You, "Controllability and stability of primary frequency control from thermostatic loads with delays," *J. Mod. Power Syst. Clean Energy*, vol. 5, no. 1, pp. 43–54, Jan. 2017.

[28] G. Angenendt, M. Merten, S. Zurmühlen, and D. U. Sauer, "Evaluation of the effects of frequency restoration reserves market participation with photovoltaic battery energy storage systems and power-to-heat coupling," *Appl. Energy*, vol. 260, Feb. 2020, Art. no. 114186.

[29] W. Liu, G. Geng, Q. Jiang, H. Fan, and J. Yu, "Model-free fast frequency control support with energy storage system," *IEEE Trans. Power Syst.*, vol. 35, no. 4, pp. 3078–3086, Jul. 2020.

[30] V. Prakash, K. C. Sharma, and R. Bhakar, "Optimal generation mix for frequency response adequacy in future power system," *Energy Built Environ.*, vol. 2, no. 3, pp. 243–250, Jul. 2021.

[31] D.-J. Lee and L. Wang, "Small-signal stability analysis of an autonomous hybrid renewable energy power generation/energy storage system. Part I: Time-domain simulations," *IEEE Trans. Energy Convers.*, vol. 23, no. 1, pp. 311–320, Mar. 2008.

[32] A. Fernández-Guillamón, E. Gómez-Lázaro, E. Muljadi, and Á. Molina-García, "Power systems with high renewable energy sources: A review of inertia and frequency control strategies over time," *Renew. Sustain. Energy Rev.*, vol. 115, Nov. 2019, Art. no. 109369.

[33] I. Pan and S. Das, "Fractional order fuzzy control of hybrid power system with renewable generation using chaotic PSO," *ISA Trans.*, vol. 62, pp. 19–29, May 2016.

[34] S. Heier, *Grid Integration of Wind Energy Conversion Systems*. Hoboken, NJ, USA: Wiley, 1998.

[35] P. K. Pathak, A. K. Yadav, and P. A. Alvi, "Advanced solar MPPT techniques under uniform and non-uniform irradiance: A comprehensive review," *J. Sol. Energy Eng.*, vol. 142, no. 4, Feb. 2020, Art. no. 040801.

[36] J. Kennedy and R. Eberhart, "Particle swarm optimization," in *Proc. Int. Conf. Neural Netw. (ICNN)*, vol. 4, Dec. 1995, pp. 1942–1948.

[37] A. Engelbrecht, "Particle swarm optimization: Velocity initialization," in *Proc. IEEE Congr. Evol. Comput.*, Jun. 2012, pp. 1–8.

[38] I. H. Altas and J. Neyens, "A fuzzy logic decision maker and controller for reducing load frequency oscillations in multi-area power systems," in *Proc. IEEE Power Eng. Soc. Gen. Meeting*, Jun. 2006, p. 9, doi: 10.1109/PES.2006.1709386.

[39] E. H. Mamdani, "Application of fuzzy algorithms for control of simple dynamic plant," *Proc. IEEE*, vol. 121, no. 12, p. 1585, 1974.

[40] T. Kerdphol, M. Watanabe, K. Hongesombut, and Y. Mitani, "Self-adaptive virtual inertia control-based fuzzy logic to improve frequency stability of microgrid with high renewable penetration," *IEEE Access*, vol. 7, pp. 76071–76083, 2019.

[41] D. Castellanos-Cárdenas, F. Castrillón, R. E. Vásquez, and C. Smith, "PID tuning method based on IMC for inverse-response second-order plus dead time processes," *Processes*, vol. 8, no. 9, p. 1183, Sep. 2020, doi: 10.3390/PR8091183.

[42] Y. Qi, H. Deng, X. Liu, and Y. Tang, "Synthetic inertia control of grid-connected inverter considering the synchronization dynamics," *IEEE Trans. Power Electron.*, vol. 37, no. 2, pp. 1411–1421, Feb. 2022, doi: 10.1109/TPEL.2021.3106948.

[43] X. S. Yang, "Firefly algorithms for multimodal optimization," in *Proc. Int. Symp. Stochastic Algorithms*, in Lecture Notes in Computer Science: Including Subseries Lecture Notes in Artificial Intelligence and Lecture Notes in Bioinformatics, vol. 5792, Oct. 2009, pp. 169–178.

SUMIT NEMA (Student Member, IEEE) received the B.E. and M.E. degrees from the Rajiv Gandhi Proudyogiki Vishwavidyalaya, Bhopal, Madhya Pradesh, India, in 2010 and 2015, respectively. He is currently pursuing the Ph.D. degree with Banasthali Vidyapith, Tonk, Rajasthan, India. His research interests include power system ancillary services planning, operation, control, and economics of power and energy systems.

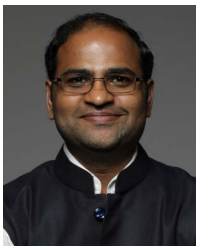

VIVEK PRAKASH (Senior Member, IEEE) received the Ph.D. degree in electrical engineering from the Malaviya National Institute of Technology Jaipur, India, in 2019. He is currently working as a Postdoctoral Research Fellow with the Faculty of Electrical Engineering and Computing, University of Zagreb, Croatia. His research interests include operations, control, and economics of power and energy systems.

HRVOJE PANDŽIĆ (Senior Member, IEEE) received the M.E.E. and Ph.D. degrees from the Faculty of Electrical Engineering and Computing, University of Zagreb, Croatia, in 2007 and 2011, respectively. From 2012 to 2014, he was a Postdoctoral Researcher with the University of Washington, Seattle, WA, USA. He is currently working as a Full Professor with the Faculty of Electrical Engineering and Computing, University of Zagreb, and the Head of the Department of Energy and Power Systems. His research interests include planning, operation, control, and economics of power and energy systems. He has been an Editor of the IEEE TRANSACTIONS ON POWER SYSTEMS, since 2019.